

Optimization of Fuel Cell Self-Humidifying System Design and SUSD Control Strategies

Tzu-Wei Kuo¹, Fang-Bor Weng¹, Chin-Hsien Cheng²

¹ Department of Mechanical Engineering & Fuel Cell Center, Yuan Ze University, Taoyuan 320, Taiwan

² Asia Pacific Fuel Cell Technologies Ltd.

*E-mail: alexkuo1303@gmail.com

Received: 2 February 2022 / Accepted: 3 April 2022 / Published: 7 May 2022

Fuel cells are widely used in vehicles and are characterized by frequent start-up/shut-down (SUSD) and dynamic load changes. These characteristics often lead to inadequate gas humidification and rapid catalyst and carbon support degradation, which can accelerate fuel cell performance deterioration. In this study, a fuel cell self-humidifying system is designed and the SUSD control strategies are optimized to address the insufficient gas humidification and rapid catalyst and carbon support degradation problems. To avoid insufficient air humidification, cooling water is allowed to flow into the wet side of the humidifier to increase the air humidity, which in turn improves the performance output of the fuel cell. The water generated by the fuel cell system is condensed and recycled into the cooling system. The adequacy of the amount of condensing water depends on the power output requirements of the system and the condensing temperature settings. Experimental results show that a condensing temperature setting of 40 °C is optimal as it satisfies the humidification water requirements for different system outputs and minimizes the power consumption of the condensing fan. The results also demonstrated a 10.4% improvement in fuel cell performance at an output power of 2.97 kW. The SUSD control strategies were optimized by changing the operating voltage, reactant concentration, and reaction time. The effect of carbon corrosion on cell performance was reduced via voltage control, vacuum pumping, and gas evacuation. After 3000 SUSD tests, the results showed a 3.6% degradation rate at the main operating power (500 mA/cm²)—a significant improvement compared with the 17.6% degradation rate of the conventional non-optimized SUSD strategy. Besides the theoretical and experimental analyses, the results of this study were integrated into a fuel cell scooter to demonstrate its feasibility. Additionally, a standard dynamic load test based on the Chinese National Standards (CNS 3105) was performed. The findings of this study could be applied to any vehicle type to enhance the performance and durability of fuel cell systems.

Keywords: Self-humidifying system, SUSD strategy, Fuel-cell powered vehicles

1. INTRODUCTION

Fuel cells are regarded as alternative sources of sustainable electricity. Proton-exchange membrane (PEM) fuel cells are suitable for operation at low temperatures and have a high energy density; thus, they are suitable for use in zero-pollution electric vehicles and stationary power stations [1,2]. Examples include lightweight cars, electric forklifts, electric vehicles, mini-trains, and bicycles [3]. Toyota launched the Mirai fuel cell vehicle in 2015, demonstrating that fuel cells have entered the commercialization phase.

In mobile vehicles, fuel cells are electrochemical power-generation systems. With frequent start-up/shut-down (SUSD) and dynamic load changes, catalyst and carbon support degradation accelerates the degradation of fuel cell performance [4], thereby hindering commercialization. Yu et al. [5] suggested that the main reason behind this is the formation of an H₂/air interface front between the anode flow field and the electrode surface during the SUSD process. This interface layer causes a hydrogen peroxide structure in the fuel cell and produces electrolysis or oxidative corrosion of the cathode. Serious performance degradation is observed in the fuel cell system without an appropriate SUSD control program after 300–500 SUSD cycles that may cause serious fuel cell degradation. Strategies such as gas purging and resistor discharge can be extended to over 1,500 cycles [6]. Perry et al. [7] proposed a voltage control method that could achieve more than 12,000 cycles without performance degradation.

Cho et al. [8] investigated the effect of carbon corrosion on durability in the context of transient changes and different microporous layer thicknesses. To reduce the effect of transients on fuel cell durability, a hybrid system can be used to maintain a stable fuel cell response by providing the power required for transient changes. Fisher et al. [9] proposed a hybrid fuel cell and Li-ion battery system for light-electric vehicle applications. The Li-ion battery provides transient requirements for the system turn on, motor power, fuel cell warmup, and motor torque. Guo et al. [10] proposed a hybrid fuel cell, lead acid battery, and supercapacitor system for electric scooters. A mathematical model was developed to simulate the performance variation of the hybrid system, and an appropriate control strategy was suggested to set the Li-ion battery at a state of charge (SOC) of 40–80% to maintain a stable output performance and achieve high-efficiency performance. Tang et al. [11] illustrated that for vehicle applications, dynamic load conditions result in fuel cell over-currents and low voltages that affect the ability of the fuel cell to conduct protons, water, and gas. The battery is used to satisfy the transient and climbing requirements of the motor, and the DC/DC converter stabilizes the voltage output and improves the efficiency of the motor. The results show that hybrid systems can maintain dynamic system stability and improve efficiency.

Fuel cell systems lead to an imbalance between water production and consumption in fuel cells without water management, resulting in negative effects such as membrane dewatering, flooding, or dilution of the reaction gas by water vapor [12].

This study develops a self-humidifying system for fuel cells and optimizes SUSD control strategies to increase the performance output of the fuel cell by directing cooling water to flow into the wet side of the humidifier to increase the air humidity and avoid membrane dewatering. Because the humidifier consumes the cooling water, the water vapor temperature at the cathode outlet is controlled to obtain condensed water and recycle it to the cooling system for water balance. The SUSD control

strategy is achieved by varying the operating voltage, reactant concentration, and reaction time to reduce the electrochemical reaction rate of carbon corrosion.

Repeated SUSD experiments were conducted to confirm the corrosion of the membrane electrode assembly (MEA) catalyst layer, and the carbon corrosion in the fuel cell was reduced. Hydrogen from the catalyst surface is removed by a resistor that changes the operating voltage. The reactant concentration is diluted by a vacuum pump, and a solenoid valve removes gas from the anode space during the reaction time. Finally, the self-humidifying system and optimized SUSD control strategies were integrated into a combined fuel cell and Li-ion-battery-powered scooter to confirm the feasibility of the developed system for vehicle applications.

2. EXPERIMENTAL METHODS

The stack used in this study was a PEM fuel cell (DuraPEM W240, provided by Asia Pacific Fuel Cell Technologies, Taiwan) with a rated power of 2.4 kW. The fuel cell stack specifications are shown in Table 1.

Table 1. Fuel cell stack specifications

Parameter	Unit	Value
Mean Area	cm ²	150
Rated Current	A	100
L × W × H	mm	239 × 152 × 192
Number of Cells	pcs	40

2.1 Fuel Cell System

The fuel cell system used in this study consists of the following: (1) hydrogen supply subsystem, (2) air supply subsystem, (3) air humidifier, (4) cooling subsystem, (5) water recycling subsystem, and (6) fuel-cell system control strategy. In this section, the various subsystems are described. The subsystems are illustrated in Figure 1, and details of the corresponding components are presented in Table 2.

Table 2. Fuel cell system components

No.	Parameter	No.	Parameter	No.	Parameter
a	PEMFC	g	Solenoid Valve (SV1)	m	Cooler
b	Air Filter	h	Gas–Water Separator	n	Water Pump
c	Air Blower	i	Hydrogen Pump	o	Condenser
d	Humidifier	j	Exhaust Valve (SV2)	p	Auxiliary Tank
e	Hydrogen Storage Tank	k	Water Jacket	q	Vacuum Pump
f	Pressure-Regulating Valve	l	Thermostat		

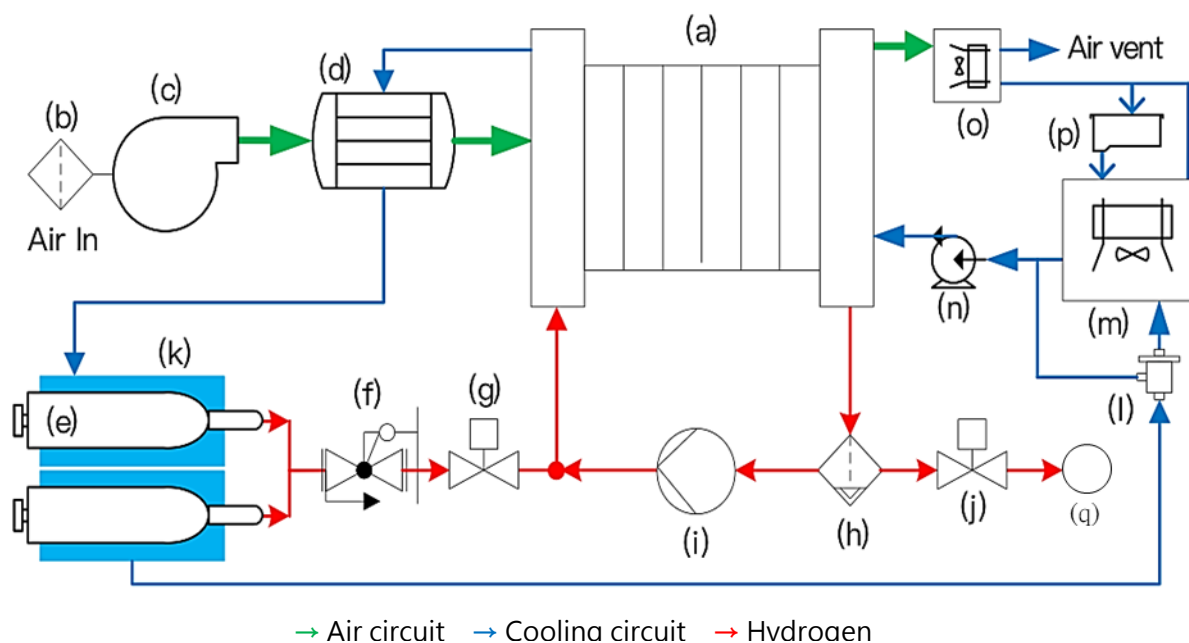


Figure 1. Block diagram of the fuel cell system

2.1.1 Hydrogen Supply Subsystem

Hydrogen was stored at a pressure of 150 psi in a hydrogen cylinder. The hydrogen cylinder contained metal hydride (AB_5). A hydrogen storage cylinder was placed in a water jacket, which is a heat-transfer device. As the fuel cell is water-cooled, the cooling water is used to transfer the heat from the electrochemical reaction of the fuel cell to the water jacket. This device heats the hydrogen storage cylinder, counteracts the heat absorption reaction during the release of hydrogen from the cylinder, and provides a stable supply of hydrogen from the cylinder. The supplied hydrogen pressure to the fuel cell can be reduced to less than 14 psi by a pressure regulator, and the hydrogen supply can be controlled by an electromagnetic valve. Water in the cathode is produced via electrochemical reaction and diffusion to the anode side, causing water to accumulate on the anode. The addition of a circulating pump to the hydrogen circuit of the fuel cell can increase the hydrogen reaction rate and alleviate the problem of flooding. At the end of the hydrogen circuit, a gas hydraulic separator can be installed to take advantage of the fact that water has a higher specific gravity than hydrogen and naturally collects at a lower level and purges to the outside (SV2).

2.1.2 Air Supply Subsystem

A blower injects oxidizer air into the cathode side, and a filter is installed in front of the blower to filter air impurities. With air provided, the blower speed is controlled via current variation using load-following technology [13]. The speed setting was based on the stoichiometric ratio, and air equivalence was range 2.5–3 [14]. A current sensor was installed in the circuit to measure the fuel cell current. When an increase in current is detected, the fuel cell controller boosts the pulse-width modulation signal to

increase the blower speed and supply the appropriate airflow. Conversely, when the current decreases, the blower speed is reduced and the maintenance speed is fixed for the basic flow (minimum flow) for cathode consumption.

2.1.3 Air Humidification Subsystem

In the case of PEM fuel cells, the system must be humidified before air enters the stack. A common form of humidification involves the installation of a humidifier in an air circuit. The interior of the humidifier is composed of membranes using a stack. [15]. The membranes separate the wet and dry circuits. Water vapor produced by the electrochemical reaction at the cathode of the fuel cell is introduced into the wet circuit of the humidifier. The water molecules diffuse through the membranes to humidify the dry air at the other end of the dry circuit; in this study, this is defined as a vapor-to-air humidification system. The advantage of the vapor-to-air humidification system is that it is simple and easy to operate; however, the humidification effect is limited to approximately 70% and the water vapor cannot be produced steadily because of the dynamic load, thus resulting in insufficient humidification capacity, increasing the likelihood of causing the fuel cell MEA to dry out. To address the problem of inadequate air humidification, in this study, instead of water vapor produced from the cathode, cooling water was introduced into the wet circuit of the humidifier. Water is transferred through a membrane inside the humidifier that humidifies the air to over 95% and brings the temperature closer to the operating temperature of the fuel cell. In this study, this humidification method is defined as a water-to-air humidification system. The humidifier used in this study is a dpoint@Px1-114.

2.1.4 Cooling Subsystem

In the present cooling system, the pump drives the cooling water into the fuel cell to carry away the heat generated by the fuel cell, and even into the wet circuit of the air humidifier. Water is transferred through a membrane to humidify and heat the air in the dry circuit. The cooling water subsequently flows into the water jacket to heat the hydrogen storage tank and maintain a warm hydrogen supply. Finally, the cooling water enters the radiator and returns to the fuel cell to complete the cooling process. A thermostat regulates the cooling-water direction before the water enters the radiator. When the water temperature is high, the hot water is in the radiator and the cooling fan is turned on. When the water is not sufficiently hot, to avoid heat loss from the radiator, the water passes through it and returns to the fuel cell. The operating temperature was maintained at 55 °C by using this cooling system.

2.1.5 Self-Humidifying System

Exchangeable vapor-to-air humidifier technology is used in typical fuel cell systems. Exchangeable humidification technology transfers water vapor from the cathode outlet to the fresh dry air at the inlet. Therefore, it does not require any water supply or storage [16]. However, water vapor

cannot be produced steadily owing to the dynamic load, resulting in insufficient humidification capacity and a tendency of the MEA to dry out. To increase the air humidity, a water-to-air humidification system was developed in this study. The cooling water on the wet side of the humidifier increases the air humidity and cathode humidification to over 95%. Because the water-to-air humidification system consumes cooling water, it is important to replenish it to avoid insufficient cooling water to cool the fuel cell. The depleted cooling water was obtained from the cathode. However, the reactant water is converted to water vapor by the heat of the fuel cell that must be condensed and recycled to replenish the cooling water consumed by the water-to-air humidification system. In this study, an additional condenser, including a temperature sensor, radiator, and cooling fan, was installed at the cathode outlet. The water vapor in the condenser and the temperature sensor controls the speed of the cooling fan to reduce the temperature. The converted condensate flows back into the cooling system to complete the self-humidifying system and maintain the cooling-water balance.

The fuel cell was tested in a laboratory under ideal conditions to assess the performance of the water-to-air humidification systems. Water vapor condensation recycling can be obtained consistently, effectively supplementing the cooling water consumption. However, in practical design, when fuel cells are used in mobile vehicles, the dynamic load and frequent SUSD may cause unstable fuel cell operating temperatures, insufficient fuel humidification, and other non-ideal conditions, making it difficult to recycle water vapor.

In this study, the experiments were set up for vapor condensation and investigate the effect of temperature. The optimum condensation temperature at different constant power outputs of the fuel cell was also investigated. The fuel cell sets a constant power of 2.0 kW, and the cooling fan cools the vapor at 50, 45, 40, 35, and 30 °C to verify the optimum condensation temperature. By collecting the condensate weight at different temperatures, an optimum condensate temperature can be obtained to replenish the cooling water and avoid unnecessary power consumption owing to the continuous operation of the cooling fan.

2.1.6 Optimization of the SUSD Logic for the Fuel Cell System

In this study, the control logic of the fuel cell system was designed to include SUSD. SUSD control strategies were implemented by varying the operating voltage, reactant concentration, and reaction time to reduce the electrochemical reaction rate of carbon corrosion. In addition, SUSD experiments were repeated to confirm the reduction of the corrosion of the MEA catalyst layer and carbon support in the fuel cells. A resistor removed hydrogen from the catalyst surface and varied the operating voltage, a vacuum pump varied the reactant concentration, and a solenoid valve removed gas from the anode space and varied the reaction time. The control logic can be written in the C programming language into a single-chip processor that can detect the value returned from each sensor every 50 ms and maintain a stable system operation through the control logic. The optimization of the SUSD control logic of the fuel cell system can be divided into two parts. The start-up and shut-down logics are shown in Figures 2 and 3, respectively.

(1) START-UP

I. The single-chip processor operates with a small Li-ion battery, providing start-up power. The single-chip system detects the pressure in the hydrogen storage tank using a pressure sensor. If the pressure is insufficient, the fuel cell system cannot be started.

II. Optimization of the start-up strategy (including opening the vacuum pump and solenoid valve SV2) will allow gas to be removed from the anode side, thereby reducing the electrochemical concentration and reaction time of the hydrogen–air interface.

III. The front end of the hydrogen regulator is at a high pressure, and the rear end is at a low pressure. If the hydrogen pressure is greater than the anode pressure, the regulator valve is adjusted to reduce the pressure. When the hydrogen regulator valve is initialized, there is a risk that the hydrogen will not drop to a low pressure owing to pressure differences that may result in overpressure. Therefore, SV2 at the end of the hydrogen supply system should be opened first, followed by solenoid valve SV1, to avoid rupture of the MEA due to differential hydrogen pressure.

IV. The blower is activated to provide minimum flow, and the single-cell voltage approaches the open-circuit voltage (OCV) or else shut down. Finally, SV2 is closed and the load relay is connected, which is supplied by the fuel cell system, when the system is stable.

V.

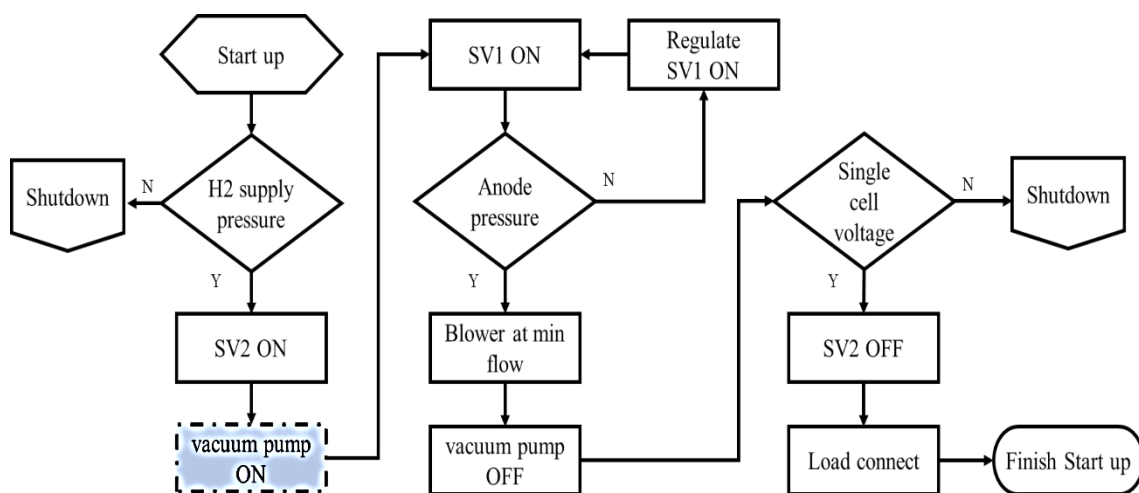


Figure 2. Optimization strategy for the start-up logic

(2) SHUT-DOWN

I. To avoid carbon corrosion of the MEA, the load relay should first be disconnected during the shutdown procedure.

II. Anode purge is conducted by opening SV2, which creates a pressure differential in the hydrogen, such that the water in the anode is drained to the outside, and then SV1 is closed. The maximum flow of the blower to purge water in the cathode is drained to the outside.

III. Optimization of the shutdown strategy (including turning on the vacuum pump) allows residual hydrogen to be extracted from the anode and reduces the hydrogen concentration.

IV. The presence of residual hydrogen and air on the MEA causes the fuel cell voltage to become an OCV. With the load off, this electrolyzes the MEA catalyst and accelerates MEA aging. Therefore, the consumption resistor is connected to vary the response voltage and the blower to supply the minimum flow to accelerate the shut-down procedure. Finally, the absence of hydrogen and the fuel cell voltage are detected, the blower is turned off, and the consumption resistor is disconnected to complete the shut-down procedure.

V.

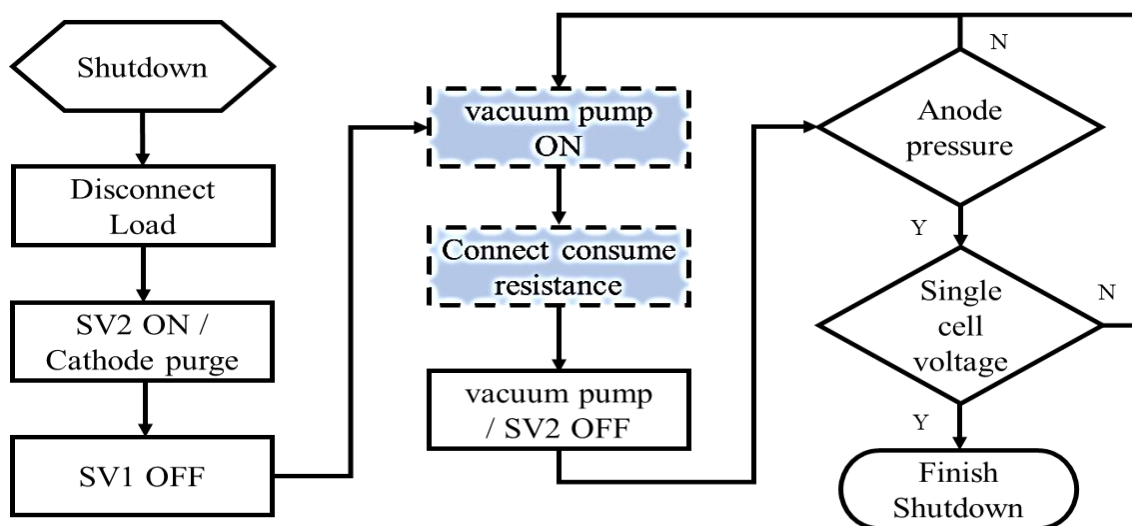


Figure 3. Optimization strategy for the shut-down logic

2.2 Hybrid Systems and Testing for the Fuel-Cell-Powered Scooter

To verify the practical application of the results presented in this study, the results of the self-humidifying system and optimized SUSD control strategies were applied to a fuel-cell-powered scooter. In this study, a Li-ion battery was integrated with a hybrid powertrain to drive the motor, and the CNS 3105 standard was used as the basis for power testing.

2.2.1 Fuel-Cell-Powered Scooter

The design, development, and production of fuel cell scooters are already on-going in Taiwan. In this study, a self-humidifying system, optimized SUSD control strategies, and hybrid power system were applied to a commercial fuel cell scooter. The scooter used was a ZES 5.0, manufactured by Asia Pacific Fuel Cell Technologies. Its specifications, along with an actual image, are shown in Table 3.

In this study, the commercially available fuel cell scooter was redesigned by installing a self-humidifying system, using optimized SUSD control strategies in the fuel cell system, and implementing the hybrid system in the fuel cell scooter. The optimized SUSD control strategies were written in the C programming language into a single-chip processor. In terms of design, the radiator was positioned at the front of the scooter and enclosed in a ventilated housing. As the scooter speed increases during actual

operation, the radiator efficiency increases owing to the increased wind speed flowing through it. Considering the weight balance and overall design of the scooter, the Li-ion battery and fuel cell system can be located underneath the scooter to increase its stability during motion. The fuel cell scooter was supplied with two 45 g @ 150 psi hydrogen storage cylinders.

Table 3. Specifications of the fuel-cell-powered scooter used in this study

Scooter Performance	Unit	Value	Fuel Cell Scooter
Maximum Speed	km/h	>45	
Acceleration (0–100 m)	s	<12	
Gradeability (12°)	km/h	20	
Range (City Mode)	km	50	
Operating Voltage	V	48	
Rated Power	kW	3.0	

When hydrogen was removed, only the hydrogen cylinders were replaced to continue operation. To increase the efficiency of the hydrogen cylinder changeover, the replacement area can be located at the rear part of the scooter to facilitate the removal of storage cylinders.

The self-humidifying system places the humidifier directly above the fuel cell to prevent heat loss. The cooling water carries heat away from the fuel cell and flows directly into the wet side of the humidifier to humidify and heat the dry air, then into the water jacket at the rear of the scooter, and finally to the radiator in the front of the scooter to complete the cooling system. A condenser comprising a temperature sensor, radiator, and cooling fan was installed at the cathode outlet underneath the fuel cell scooter. The water vapor from the cathode outlet is cooled to the condensate that is stored in a small water tank. When the cooling water circuit is running low, the condensate is pumped out by a mini-pump and recycled into a secondary tank to replenish the cooling water, complete the self-humidifying system, and maintain the cooling water balance.

2.2.2 Hybrid Systems and Testing for the Fuel-Cell-Powered Scooter

The hybrid system can be divided into the Li-ion battery mode and fuel cell mode. The control strategy is illustrated in Figure 4. The control strategy for the Li-ion battery mode is based on a state of charge (SOC) of 40–80% [17]. When the SOC exceeds 40%, the fuel cell is not activated, and the Li-ion battery provides the main power to drive the motor. When the SOC is less than 40%, the fuel cell is in the start-up mode, with the fuel cell providing the main power, driving the motor, and charging the Li-ion battery at low loads. When the fuel cell system is activated, the Li-ion battery is charged, which gradually increases the SOC. When the SOC exceeds 80%, the fuel cell system is shut down and switches to battery mode to drive the motor.

The hybrid system consists of a fuel cell system, DC/DC booster, Li-ion battery, DC/DC converter, motor controller, and hub motor. The system block diagram is shown in Figure 5 and its specifications are presented in Table 4. The Li-ion battery drives the motor at 48 V @ 40 Ah via a main relay. The DC/DC converter is fed from the VBUS at 40–54 V and back to 12 V to drive the fuel cell components (e.g., blower, pump, and valve) to start the fuel cell system. The 24-V fuel cell system requires a DC/DC converter to boost the voltage to 40–54 V. The booster voltage output is subsequently used to regulate and control the fuel cell output at a constant power of 2 kW to drive the motor and charge the Li-ion battery at low loads. In this study, the CNS 3105 vehicle model (Figure 6) was used as the basis for power testing [18,19].

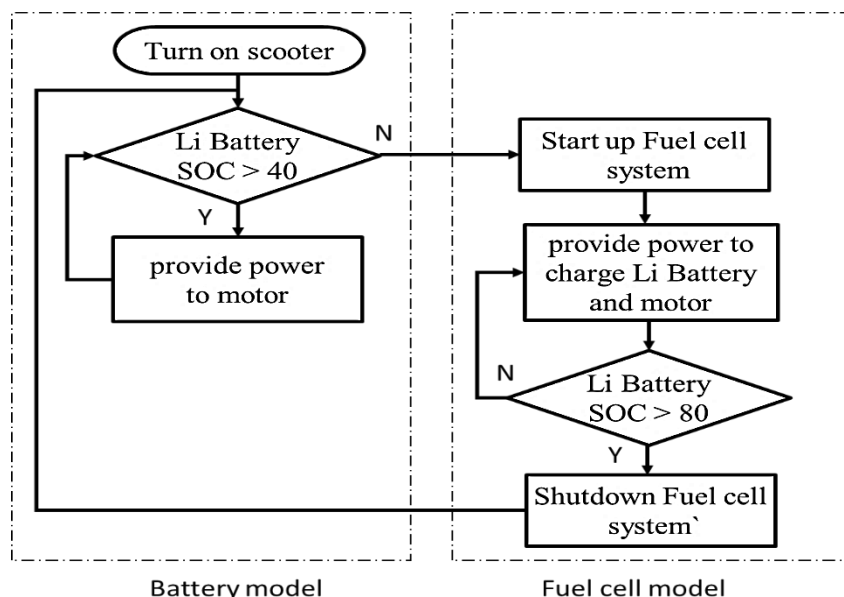


Figure 4. Control strategy of the fuel cell hybrid system

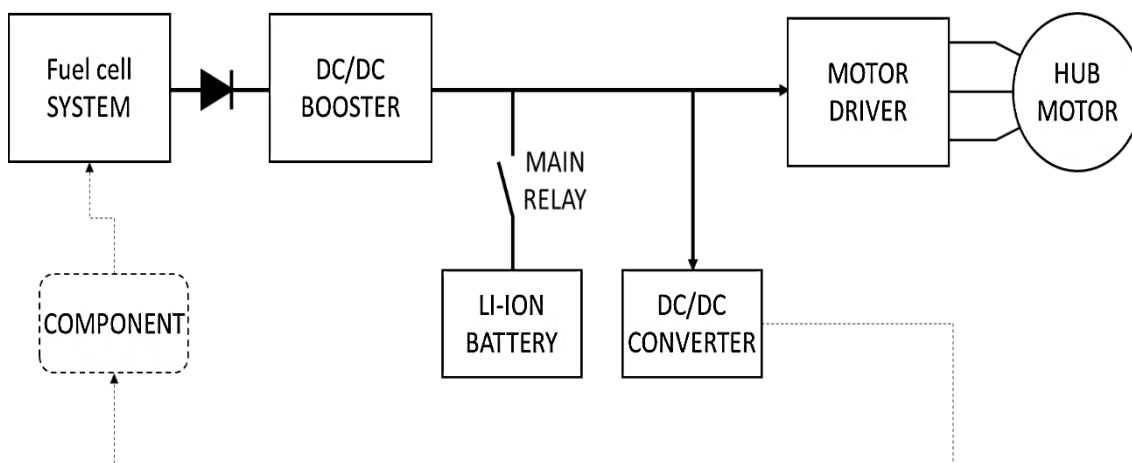


Figure 5. Block diagram of the fuel cell hybrid system

Table 4. Component specifications of the fuel cell hybrid system

System block	Parameter	Unit	Value
Fuel Cell System	operating voltage	V	25
	rated power	kW	3.0
DC/DC Booster	input voltage	V	20–36
	output voltage	V	40–54
	rated power	kw	3.0
Li Ion Battery	operating voltage	V	48
	capacity	Ah	40
DC/DC Converter	input voltage	V	40–54
	output voltage	V	12
	rated power	kw	1.0
Motor Driver	operating voltage	V	48
	rated power	kW	3.0
Hub Motor	rated power	kW	3.0
Component	fuel cell control	V	12

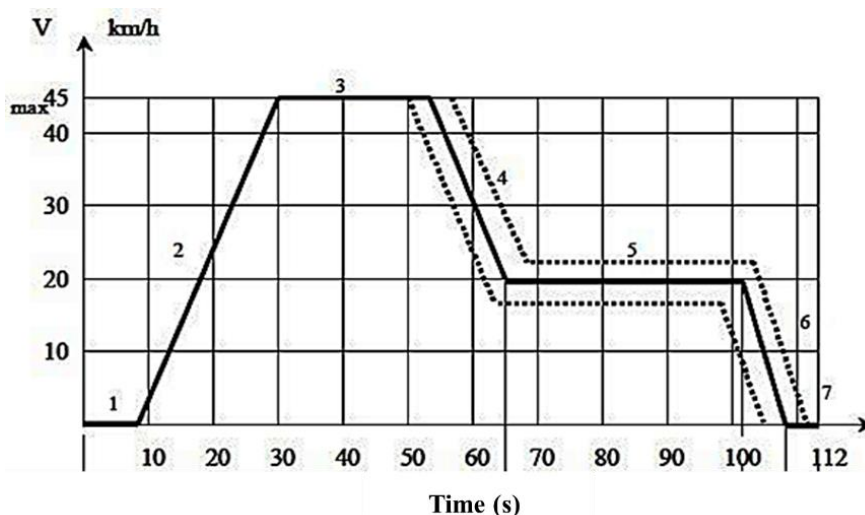


Figure 6. CNS 3105 vehicle model used in this study [19]

3. RESULTS AND DISCUSSION

3.1 Fuel Cell System Performance

The water molecules produced by the cathode were exchanged in the membrane for humidification. However, relying solely on cathode-reaction water molecules is not sufficient to humidify the membrane as a mass exchanger, particularly at low loads. Therefore, the fuel cell must be further humidified by an additional humidifier. The water-to-air humidification system designed in this study exhibits a better humidifier performance (>95% RH) than conventional vapor-to-air humidifiers,

which have a humidification capacity of approximately 70% RH. The use of a water-to-air humidification system can increase the cathode humidification capacity by 35% and improve the overall fuel cell performance. The operating conditions of the fuel cell system were a hydrogen equivalence of 1.2, air equivalence of 3.5, anode pressure of 14 psi, and operating temperature of 55 °C. A cell current density of 800 mA/cm² demonstrated a maximum power of 2.97 kW and an operating voltage of 24.74 V, as shown in Figure 7.

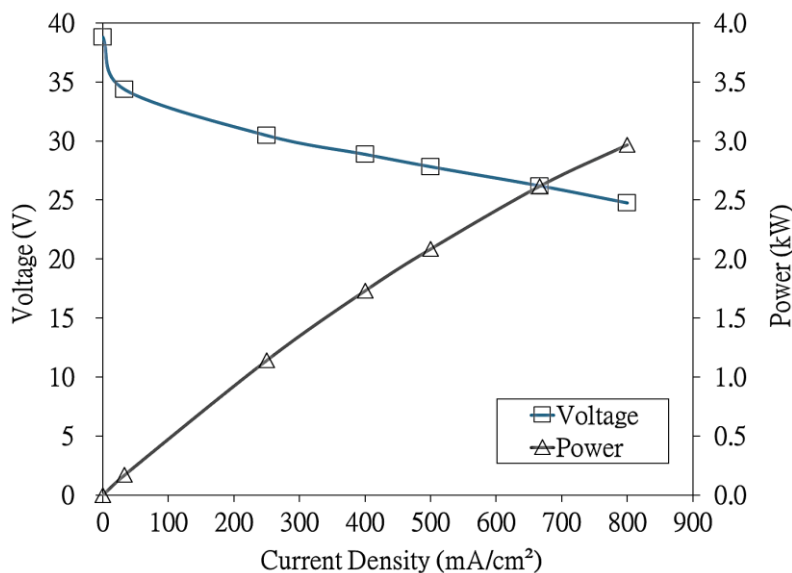


Figure 7. Fuel cell polarization curves when using the proposed self-humidifying system

A fuel cell system under the same operating conditions as the vapor-to-air humidifier was applied to forklifts [20]. A comparison of the vapor-to-air and water-to-air polarization curves is shown in Figure 8. At a low current density of 40 mA/cm², conventional humidifiers are unable to improve their humidification performance because of insufficient water reacting with the cathode, resulting in a voltage of 33.2 V. Humidifiers based on water-to-air humidification systems do not suffer from insufficient water production at the cathode, which affects their humidifying capacity. Therefore, the performance is improved at low current densities, exhibiting a voltage of 34.35 V.

The performance enhancement rate of the water-to-air humidification system at different current densities was calculated, as shown in Figure 9. At 250–500 mA/cm², the water-to-air humidification system outperformed the vapor-to-air humidifier by approximately 4%, which is not significant, mainly because the humidification capacity of the vapor-to-air humidifier was sufficient to supply the electrochemical reaction of the fuel cell. At an optimum operating voltage of 0.65 V and a total voltage of 26 V, the fuel cell under vapor-to-air humidification exhibited a current density of 580 mA/cm² @ 2.25 kW. In the water-to-air humidification system, the current density of the fuel cell was 685 mA/cm² @ 2.70 kW. When the corresponding current density of the fuel cell system was 800 mA/cm², the performance of fuel cell under vapor-to-air humidification was 22.4 V @ 2.69 kW. The fuel cell performance of the water-to-air humidification system was 24.74 V @ 2.97 kW. These results demonstrated a 10.4% power output improvement under water-to-air humidification.

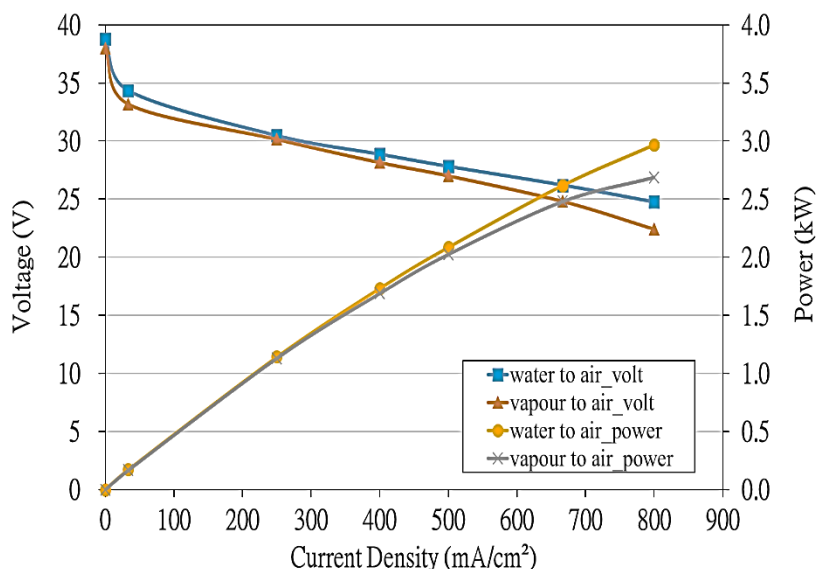


Figure 8. Polarization curve comparison between the vapor-to-air and water-to-air humidification

At high current densities, water produced at the cathode diffuses unevenly to the anode. The MEA of the anode, particularly at the inlet, loses water and dries out. Although the cathode produces water, facilitating the transfer of protons within the polymer membrane, at a high current density, the MEA dries out near the cathode inlet because of the large amount of air required to operate at high current densities, resulting in a significant increase in the electrical resistance. In this study, by using the water-to-air humidification system, the air humidity exceeded 95%, avoiding the risk of drying out the MEA with large amounts of air at high current densities. To properly assess the impact of the water-to-air humidification system used in this study, these results were compared with those of previous studies. A previous study investigated the performance of commercial Ballard MK5-E fuel cell stacks at different temperatures (24–72 °C). At an operating temperature of 56 °C and a current density of 600 mA/cm², the reaction voltage was 0.64 V [21]. Murugesan et al. [22] demonstrated the effect of water flooding on the performance of Ballard MK5 fuel cell stacks. Under light flooding and a working temperature of 72 °C, the polarization curve voltage at 600 mA/cm² were 0.72 V. Another study investigated the performance of an electric vehicle with an integrated 7-kW fuel cell system for the main energy, a LiPo battery (40 Ah) for auxiliary energy and brake recharge, and an ultracapacitor (350 F) to provide booster energy for acceleration. The fuel cell single voltage at a current density of 700 mA/cm² was 0.62 V [23]. A triple hybrid system comprising a PEMFC, lead-acid battery, and an ultracapacitor has also been investigated. The fuel cell power of that system was approximately 9 kW, and the cell working voltage was approximately 0.59–0.74 V. The fuel cell single voltage at a current density of 550 mA/cm² was 0.66–0.71 V [24].

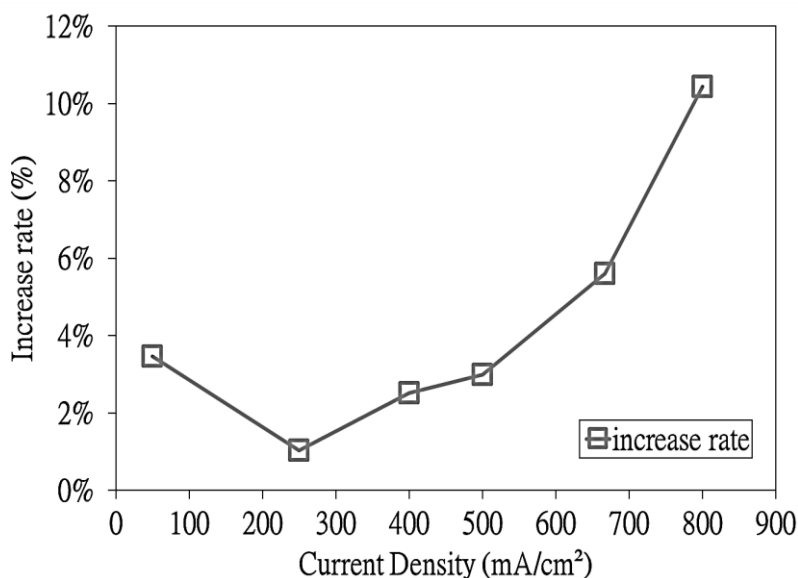


Figure 9. Performance improvement due to the proposed water-to-air humidification system

3.2 Condensate Temperature Experiment

The water-to-air humidification system is connected in series to the humidifier wet-air flow path through the cooling system that replaces the traditional wet-air flow path from the cathode outlet into the humidifier. The diffusion drive of the water molecule concentration difference allows the humidification of dry air. Water molecules force the diffusion of humidified fresh air, which leads to cooling water consumption. Appropriate replenishment is necessary to avoid the risk of fuel cell overheating owing to cooling water loss. This section discusses the energy consumption of the condenser and the condensing temperature optimization control.

3.2.1 Condenser Energy-Consumption Test

The water vapor from the fuel cell cathode outlet passes through the condenser and cooling fan, and the condensing temperature is detected by a temperature sensor at the condenser outlet to control the speed of the cooling fan to achieve condensation. When the condensing temperature exceeds a set value, increasing the speed of the cooling fan causes the water vapor to condensate, replenishing the cooling water.

For mobile vehicles, the condenser at the cathode outlet can be used to obtain sufficient condensate to replenish the cooling water. However, the cooling fan consumes additional power and hydrogen. Therefore, to achieve minimum hydrogen consumption and sufficient water recycling, it is necessary to optimize the condensate temperature control. In this study, the energy consumption of the cooling fans was analyzed at different condensing temperatures (25, 30, 35, 40, 45, and 50 °C). As shown in Figure 10, the maximum power consumption required at a condensing temperature of 25 °C was 164.7 W. However, at 50 °C, the minimum power consumption was 45.9 W. The lower the condensing temperature, the higher the fan speed required to control the condenser, which results in a lower

condensing temperature and higher power consumption, which in turn affects the amount of hydrogen used in mobile vehicles.

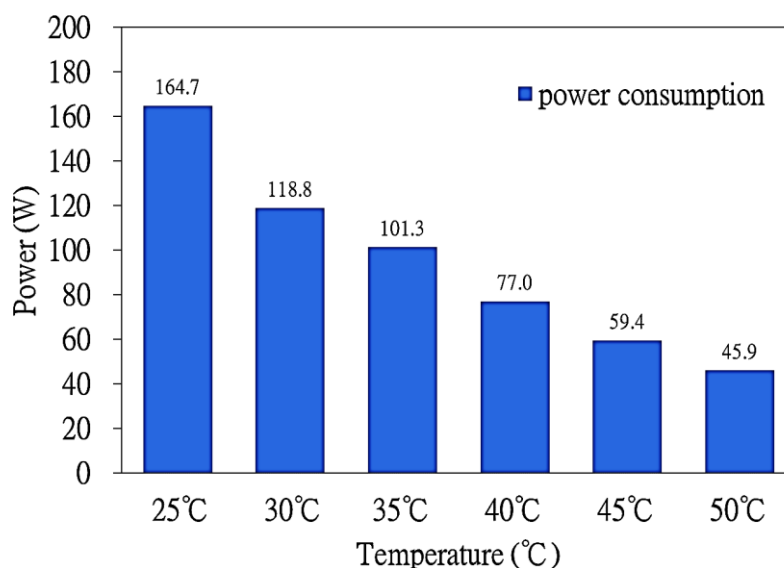


Figure 10. Condenser power consumption

3.2.2 Condensing Temperature Optimization Control Analysis

In this section, the experimental results for different constant powers are discussed. The condensation temperature of the water vapor at the cathode outlet was controlled, and the effect of the condensation temperature on the amount of water produced is discussed to analyze the condensation temperature at which water consumption can be balanced to avoid additional energy consumption in the condenser and to reduce the amount of hydrogen used.

First, the fuel cell system output was set to a constant power of 1 kW and the condensation temperatures were set to 30, 35, 40, 45, and 50 °C. After 1 h of continuous operation, the condensate weight was measured. Thereafter, the constant power was gradually increased at 0.4-kW intervals to 1.4, 1.8, 2.2, 2.6, and 3 kW. The difference in water production at different condensate temperatures for each constant power load was analyzed, and the results are shown in Figure 11. The experimental results show that, as long as the condensing temperature is set above 45 °C, the condensate weight at any given power does not balance the consumption requirements of the water-to-air humidification system. If the condensing temperature is set to 40 °C, a constant power of at least 1.4 kW is required for the condensate to balance the consumption of the water-to-air humidification system. If the condensing temperature is 35 °C, a constant power of 1.0–3 kW will balance the consumption of the water-to-air humidification system; however, the relative power consumption of the condenser will increase.

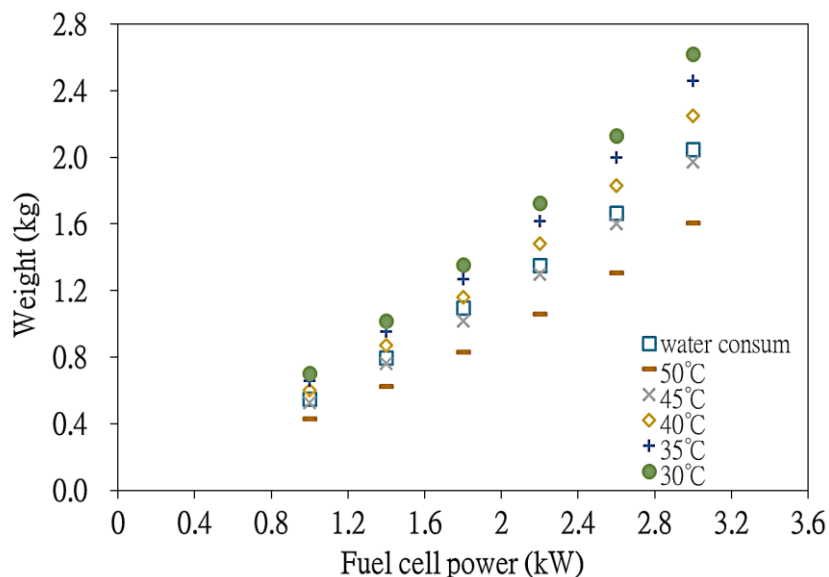


Figure 11. Water production and consumption under different condensing temperatures at different constant power loads

3.2.3 Verification of the Optimum Condensing Temperature Parameters

The operating power of the fuel cell scooter was set at 2.0 kW as the test condition, and it was verified that the optimum condenser temperature at the outlet of the cathode was 40 °C. The condensate temperature was set to 25, 30, 35, 40, 45, and 50 °C, and the condensate weight was recorded every 10 min. The experimental results show that the cumulative 1-h condensate weights (Figure 12a) are 1.7, 1.6, 1.5, 1.4, 1.2, and 1.0 kg, respectively. The power consumptions of the condenser, as percentages of a constant power of 2.0 kW (Figure 12b), are 8.24%, 5.94%, 5.06%, 3.85%, 2.97%, and 2.30%, respectively, for the different condensing temperature settings.

The data show that the condensate weight increases linearly in equal proportions under all temperature conditions. The weight of the water produced by a condensate water temperature of 25–40 °C exceeds the cooling water consumption of the water-to-air humidification system that can balance the cooling system; however, it cannot be balanced at 45–50 °C. The condensate temperature was optimized to 40 °C, and a condensate weight of 1.4 kg/h was sufficient for compensation. To avoid unnecessary hydrogen consumption, it was not necessary to set the condensate at 25–35 °C.

Experimentally, it takes 0.3 h before the condensate production at 40 °C begins to exceed the cooling water consumption of the water-to-air humidification system. Therefore, the fuel cell system needs to operate for at least 0.3 h after start-up for water recycling to balance the cooling system; otherwise, the condensate temperature must be reduced below 30 °C to ensure that the condensate fully balances the cooling system, but this increases the condenser consumption and affect the amount of hydrogen used. Therefore, the system design should consider the fuel cell operating time to avoid imbalance in the water-to-air humidification system.

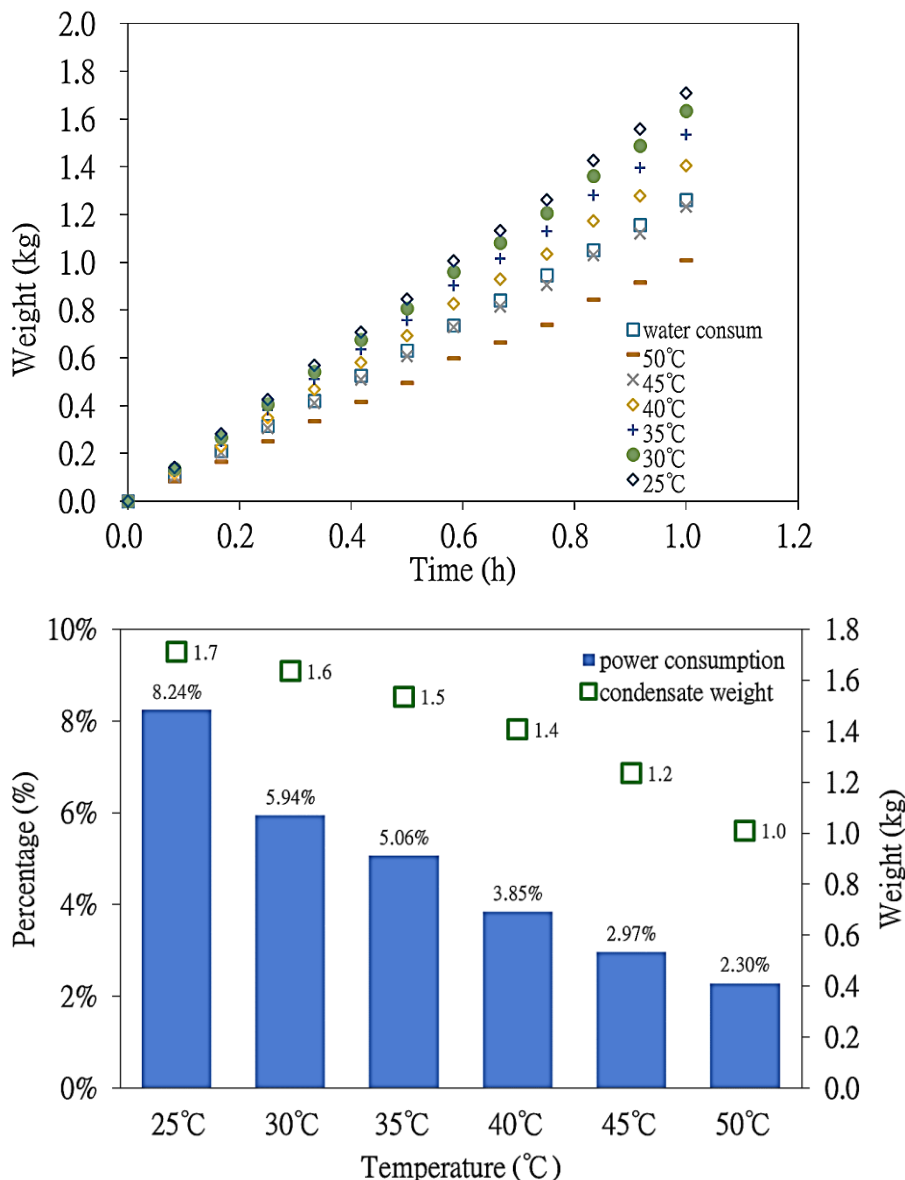


Figure 12. (a) Condensate weight for condensate temperature variation. (b) Condenser power consumption and condensate weight at a constant power of 2.0 kW

3.3 Optimization of the SUSD Control Strategies

The aim of the SUSD strategy for fuel cells is to mitigate the carbon corrosion problem caused by uneven fuel and voltage distribution in the stack. The optimized control strategy was applied to the fuel cell system during 3000 SUSD cycles, and its performance was compared with that of the conventional non-optimized SUSD strategy. The performance curves are shown in Figure 13. This study uses resistance consumption to control the response voltage and to avoid the phenomenon of the fuel cell maintaining an OCV for long periods during shut-down. This voltage phenomenon can cause catalyst buildup or carrier corrosion and can enable a speedy shut-down procedure. In practice, fuel cell scooters operate mainly at medium power (27.8 V: 0.69–0.7 V @ 500 mA/cm²). The optimized strategy

voltage is reduced from 27.8 to 26.8 V (3.6% degradation) relative to the conventional strategy voltage reduction from 27.8 to 22.9 V (17.6% degradation). Perry et al. [7] proposed that voltage control during SUSD procedures decrease cell performance by approximately 5% in the mid-power region after 10,000 cycles. With a high current range of 800 mA/cm², the conventional shut-down strategy caused significant performance and electrochemical degradation after 3000 cycles. Therefore, the SUSD strategy through vacuuming, voltage control, and gas evacuation is key to reducing the aging phenomenon. These results were compared with those of previous studies. Three fuel cell operation modes under SUSD cycles are provided, and the durability evaluation time is shortened through different operation modes. After 600 cycles, 2 h of constant power operation, and a 2-h load off, cell performance decreased by approximately 16%. This result describes the limit at the anode after which irreversible performance deterioration is caused due to carbon corrosion [25]. The SUSD strategy for a high-temperature PEMFC and continuous operation for more than 1500 cycles has been investigated. During the start-up procedure, hydrogen was initiated at the anode side and subsequently, air flowed into the cathode after 30 s. In the shut-down procedure, with the load off and the air flow shut off, the voltage was reduced to zero and the nitrogen was switched to the anode side. A higher degradation rate of 133 μV/cycle was observed at an OCV [26].

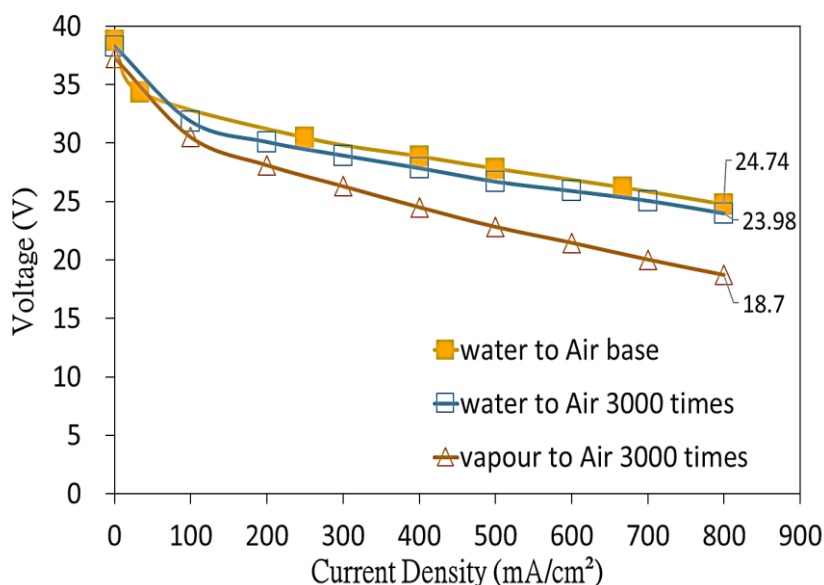


Figure 13. Performance comparison between the optimized and non-optimized conventional strategies

3.4 Fuel-Cell-Powered Scooter Test Results

A self-humidifying system and optimized SUSD control strategies can be integrated into fuel-cell-powered scooters to ensure their performance stability. In addition, it was possible to measure the condition of the unit at a stable output of 2 kW. These measurement results are shown in Figure 14. A constant power output of 27.8 V @ 2.08 kW was obtained at a current density of 500 mA/cm². The voltage of every cell is in the range of 0.69 to 0.70 V.

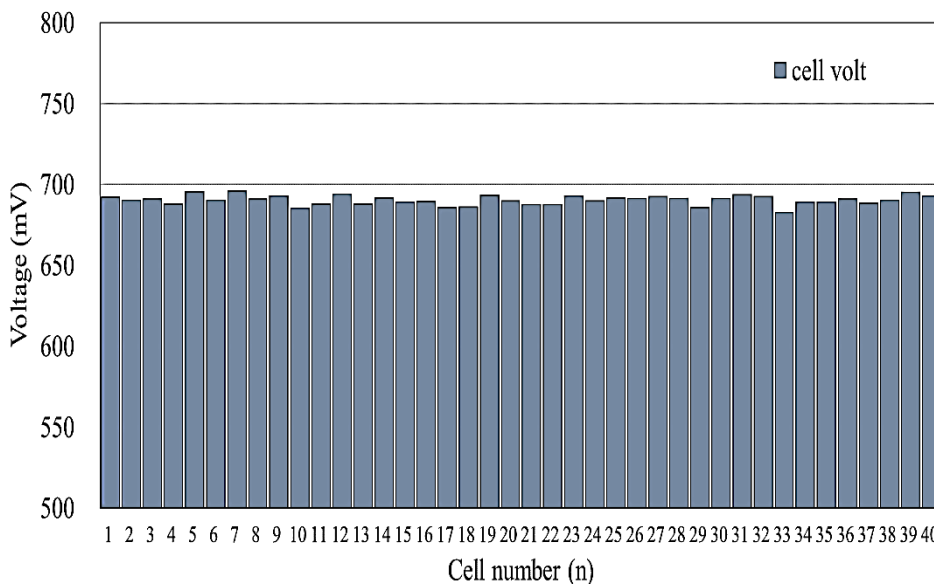


Figure 14. Fuel cell voltage variation at a constant power load

The dynamic performance of the fuel cell scooter was tested in the CNS 3105 driving mode. The maximum motor power requirement for the fuel cell scooter was 2.2 kW, and the maximum speed was 45 kph. The hybrid power strategy used in this study uses two power supplies. The Li-ion battery directly provides the initial power to the electrical system and drives the motor. The Li-ion battery voltage gradually decreases in the driving mode. The SOC decreases from 80% to 40% and triggers the fuel cell start-up. The fuel cell drives the motor at a constant power of 2.0 kW via a DC/DC booster. A Li-ion battery can be charged when the motor load demand is low. As the charging time increases, the Li-ion battery voltage and SOC gradually increase. When the SOC is 80%, the fuel cell system is shut down, the Li-ion battery charging mode is stopped, and the Li-ion battery continues to supply the motor power consumption. The Li-ion battery SOC and DC bus voltages are shown in Figure 15.

The test results show that the proposed self-humidifying system and SUSD control strategies can be adopted in a fuel cell scooter. Under a dynamic load, if the vapor-to-air humidification system is used, water vapor will not be generated stably; this will result in insufficient humidification capacity and will easily cause the fuel cell MEA to dry out. With the aid of a water-to-air humidification system, the cooling water immediately humidifies the cathode fuel without affecting the humidification capacity owing to load variations or failure to reach the operating temperature. An immediate power supply from the fuel cell to the dynamic load is maintained. This energy control logic allows the fuel cell voltage to be output in a stable manner, it also protects the fuel cell.

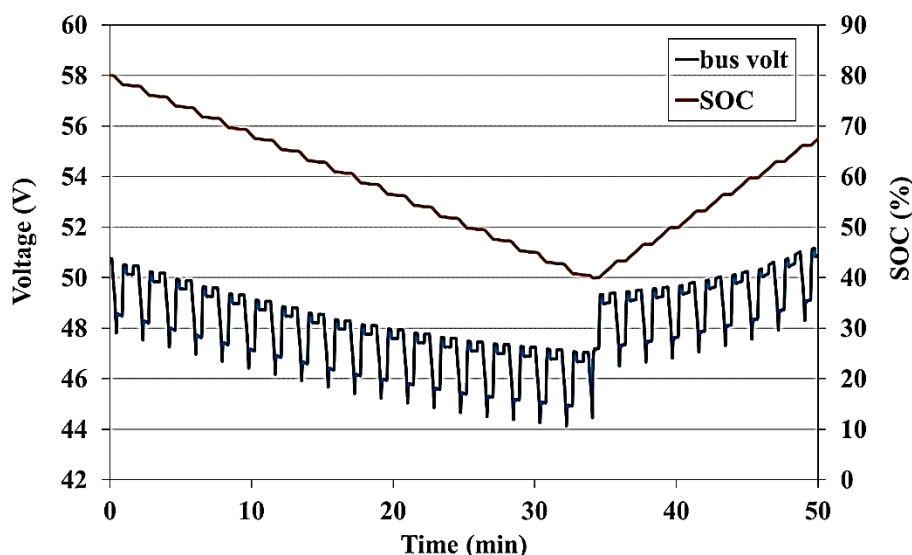


Figure 15. Li-ion battery SOC and DC bus voltage curves

4. CONCLUSION

To address the problems of inadequate gas humidification and rapid aging of catalytic carbon carriers in vehicle applications owing to frequent SUSD and dynamic load changes, a fuel cell self-humidifying system was developed and SUSD control strategies were optimized in this study. The developed self-humidifying system and optimized SUSD control strategies have been experimentally proven to improve the fuel cell performance and mitigate the aging problem caused by frequent on/off cycles. The optimized SUSD control strategies reduce the occurrence of carbon corrosion via resistance (by varying the operating voltage), vacuum-pumping (by varying the reactant concentration), and flushing the gas (by varying the reaction time). The self-humidifying system and SUSD control strategies could be applied to fuel-cell-powered vehicles. Based on experimental results, the main findings of this study can be summarized as follows.

- The operating temperature of the fuel cell was maintained at 55 °C, and the condensation temperature was maintained at 40 °C. A difference of 15 °C between the two temperatures provides sufficient condensate to compensate for the cooling water consumed during operation.
- As the current density increased, the water-to-air humidification system significantly improved the performance of the fuel cell. At 680 mA/cm², the improvement was 5.6%. At 800 mA/cm², the fuel cell output of the water-to-air humidification system was 2.97 kW. This is an effective 10.4% increase in the output power compared with the 2.69-kW output power of the vapor-to-air humidification system.
- SUSD experiments performed for 3000 cycles confirmed reduction the carbon corrosion of MEA catalyst layer in the fuel cells.
- A 3.6% degradation rate at the main operating power (500 mA/cm²) represents a significant 17.6% improvement over the conventional non-optimized SUSD strategy.
- In the hybrid system, the fuel cell output at a constant power of 2 kW protected the fuel cell from

dynamic loads that could affect its performance.

- The self-humidifying system and optimized SUSDC control strategies were integrated into a fuel-cell-powered scooter. It was verified that under CNS 3105 test conditions, the fuel cell exhibited a steady 2-kW output and was not affected by the dynamic motor load.

ACKNOWLEDGEMENT

We would like to thank Asia Pacific Fuel Cell Technologies, Ltd. (APFCT) and the Fuel Cell Center at Yuan Ze University for their technical and financial assistance in making this project possible.

References

1. D. T. Santa Rosa, D. G. Pinto, V. S. Silva, R. A. Silva and C. M. Rangel, *Int. J. Hydrogen Energy*, 32 (2007) 4350.
2. G. Hoogers, Fuel cell Technology-Handbook, *CRC Press*, (2002) Boca Raton, United States.
3. F. Barreras, M. Maza, A. Lozano, S. Bascónes, V. Roda, J. E. Barranco, M. Cerqueira and A. Vergés, *Int. J. Hydrog. Energy*, 37 (2012) 15367.
4. F.B. Weng, T.W. Kuo, and M.H. Chung, System mitigated strategies of start/stop procedures on fuel cell degradation, *Chem. Eng.*, Taipei, Taiwan, 2017, 63.
5. Y. Yu, H. Li, H. Wang, X. Z. Yuan, G. Wang and M. Pan, *J. Power Sources*, 205 (2012) 10.
6. F. Al-Saleh, V. Buday, O. Klein, T.V. Unwerth and S. Scholl, *J. Fuel Cell Sci. Technol.*, 11 (2014) 011001.
7. M. L. Perry, T. W. Patterson and C. Reiser, *ECS Trans.*, 3 (2006) 783.
8. J. Cho, J. Park, H. Oh, K. Min, E. Lee and J. Y. Jyoung, *Appl. Energy*, 111 (2013) 300.
9. P. Fisher, J. Jostins, S. Hilmanen and K. Kendall, *J. Power Sources*, 220 (2012) 114.
10. L. Guo, K. Yedavalli and D. Zinger, *Energy Convers. Manag.*, 52 (2011) 1406.
11. Y. Tang, W. Yuan, M. Pan and Z. Wan, *Appl. Energy*, 88 (2011) 68.
12. J. J. Hwang and H. S. Hwang, *J. Power Sources*, 104 (2002) 24.
13. Y. Zhu and K. Tomsovic, *Electr. Power Syst. Res.*, 62 (2002) 1.
14. G. Squadrito, G. Maggio, E. Passalacqua, F. Lufrano and A. Patti, *J. Appl. Electrochem.*, 29 (1999) 1449.
15. S. K. Park, E. A. Cho and I. H. Oh, *Korean J. Chem. Eng.*, 22 (2005) 877.
16. J. J. Huang, Fuel Cell, *Tsang Hai Book Publishing Co.*, (2017) Taipei, Taiwan.
17. L. Guo, K. Yedavalli and D. Zinger, *Energy Convers. Manag.*, 52 (2011) 1406.
18. P. T. Chen, D. J. Shen, C. J. Yang and K. D. Huang, *Appl. Sci.*, 9 (2019) 1787.
19. Chinese National Standards (CNS), Method of Test Fuel Consumption for Motorcycle CNS 3105: D3029, (2001), Taipei, Taiwan.
20. C. Y. Hsieh, X. V. Nguyen, F. B. Weng, T. W. Kuo, C. Y. Lee and A. Su, *Int. J. Electrochem. Sci.*, 12 (2017) 6266.
21. F. Laurencelle, R. Chahine, J. Hamelin, K. Agbossou, M. Fournier, T. K. Bose and A. Laperrière, *Fuel Cells*, 1 (2001) 66.
22. K. Murugesan and V. Senniappan, *Int. J. Electrochem. Sci.*, 8 (2013) 7885.
23. Inayati, H. T. Waloyo, M. Nizam and H. Saidi, Model-Based Simulation for Hybrid Fuel Cell/Battery/Ultracapacitor Electric Vehicle, *ICEVT*, Surakarta, Indonesia, 2018, 112.
24. T. M. Keränen, H. Karimäki, J. Viitakangas, J. Vallet, J. Itonen, P. Hyöttylä, H. Uusalo and T. Tingelöf, *J. Power Sources*, 196 (2011) 9058.
25. S. J. Bae, S. J. Kim, J. I. Park, C. W. Park, J. H. Lee, I. Song, N. Lee, K. B. Kim and J. Y. Park, *Int. J. Hydrog. Energy*, 37 (2012) 9775.

26. A. Kannan, A. Kabza and J. Scholta, *J. Power Sources*, 277 (2015) 312.

© 2022 The Authors. Published by ESG (www.electrochemsci.org). This article is an open access article distributed under the terms and conditions of the Creative Commons Attribution license (<http://creativecommons.org/licenses/by/4.0/>).